energies

MDPI

Article

MSR Fuel and Thermohydraulic: Modeling of Energy Well Experimental Loop in TRACE Code

Giacomo Longhi [1], Guglielmo Lomonaco [2,3,*], Tomáš Melichar [1] and Guido Mazzini [1,*]

[1] Centrum Výzkumu Řež s.r.o. (CVŘ), 250 68 Husinec-Řež, Czech Republic; giacomo.longhi@cvrez.cz (G.L.); tomas.melichar@cvrez.cz (T.M.)
[2] GeNERG, DIME, Università di Genova, 16145 Genova, Italy
[3] INFN, Sezione di Genova, 16146 Genova, Italy
* Correspondence: guglielmo.lomonaco@unige.it (G.L.); guido.mazzini@cvrez.cz (G.M.)

Abstract

The transition toward carbon-neutral energy systems has revived interest in nuclear technologies, particularly small and micro modular reactors (SMRs and MMRs) as flexible, safe and efficient alternatives to conventional large-scale power plans. In the Czech Republic, Centrum výzkumu Řez (CVŘ) is developing Energy Well (EW), a molten salt-cooled micro modular reactor concept employing FLiBe (Fluoride Lithium Beryllium) as primary and secondary coolant and a supercritical CO_2 (sCO_2) tertiary loop. A dedicated experimental facility was built to reproduce EW operating conditions and provide critical data on thermohydraulic behavior, fuel properties and heat-transfer mechanisms. This paper presents the development and assessment of a TRACE (TRAC/RELAP Advanced Computational Engine) model of the experimental facility, including specific methodologies for the main heater and the heat exchanger. Model accuracy was assessed through comparison with experimental commissioning data. The simulations demonstrated overall model consistency, especially regarding the heat exchanger and the main heater general performances, while some discrepancies were observed inside the main heater graphitic core. Other discrepancies were observed along the loop, mainly resulting from modeling simplifications and lack of information regarding certain experimental loop phenomena. In particular, the pressure calculation showed large inconsistencies mainly connected to the complexity of pressure measurements in molten salt circuits and the lack of specific head loss correlations. This study also helped identify broader issues in both the code (persistent error in generating CO_2 property tables and instabilities resulting from FLiBe interactions with non-condensable gases) and the experimental loop (defect in the heat exchanger filling and uncertainties on sensors location), also contributing to resolving sensor-related inconsistencies in the facility. Results confirm TRACE as a reliable tool for modeling molten salt systems, regarding the temperature distribution and the heat transfer. However, depending on the specific experimental case, this paper introduces specific limitations, such as some inconsistencies in the pressure drops distribution, in order to support the future development of TRACE code. Beyond technical advances, this work provides unique experimental data and fosters international collaboration in advancing SMR and molten salt reactor technologies.

Keywords: MSR; Energy Well; TRACE; FLiBe; SMR; CO_2 property tables

Academic Editors: Artur Blaszczuk and Enrico Zio

Received: 23 September 2025
Revised: 11 February 2026
Accepted: 12 February 2026
Published: 21 February 2026

1. Introduction

In recent years, the urgency to transition toward a carbon-neutral economy has become a cornerstone of European policy. In response to the dual challenges of achieving climate neutrality and ensuring energy security, European countries are diversifying their energy mix. While renewables remain central to this transition, nuclear energy is being reconsidered for its ability to provide stable, low-carbon electricity. Small and micro modular reactors (SMRs and MMRs) are being explored as a promising alternative to conventional large-scale nuclear power plants, offering advantages in flexibility, safety and installation speed [1,2].

The Czech Republic is actively investing in SMRs, both through the deployment of existing designs and the development of innovative concepts [3]. Among them, within a consortium led by Centrum výzkumu Řež (CVŘ), a new concept of MMR cooled by molten salt is under development. Energy Well (EW) is a Fluoride Salt-Cooled High-Temperature MMR concept of 20 MW(t) [4], designed for decentralized energy production, with a strong emphasis on safety, efficiency and sustainability [5,6].

Molten salt reactors belong to the Generation IV class of nuclear reactor designs under development. They are intended to operate at high temperatures (up to 700–750 °C), with the fissile material dissolved in a molten salt mixture, which increases efficiency. They offer several attractive features, such as high thermal stability and boiling point, strong irradiation resistance, the possibility of reusing fuel containing actinides, low operational pressure and many others, all contributing to significant safety and cost advantages [7,8].

A relevant class of salt-based reactors is represented by Fluoride Salt-Cooled High-Temperature Reactors. Unlike classic molten salt reactors, they mostly employ solid TRISO (Tri-Structural Isotopic) as fuel while using low-pressure fluoride salts as primary coolants. TRISO fuel particles consist of microscopic uranium-bearing kernels encapsulated in three carbon- and ceramic-based coating layers. These very small and highly robust particles act as a containment system themselves, providing exceptional retention of fission products and resistance to irradiation. This hybrid approach combines the high-temperature performance typical of molten-salt technology with the robust fuel integrity and passive safety characteristics of TRISO fuel [9,10].

To this group belongs the EW design, which uses molten salt FLiBe as both its primary and secondary coolant, while the tertiary circuit employs a supercritical CO_2 (sCO_2) loop to enhance efficiency. These innovations make EW suitable for applications such as remote industrial or district heating, hydrogen production and electricity generation [4].

One of the key steps toward realizing the Energy Well project is the experimental evaluation of its thermohydraulic properties, focusing on the fuel behavior and the heat transfer between FLiBe and supercritical CO_2. This evaluation is crucial for the design and optimization of components such as the reactor vessel and the heat exchangers. To this end, a specialized experimental loop was developed to simulate EW operational conditions, designed and built under the Czech national project Energy Well (TAČR project number TK02030125) [11]. One of its main tasks is also to provide data for simulating EW flow regimes, particularly fuel and heat exchange, in order to assess the capabilities of computational codes [6].

This paper focuses on the development of a model of the experimental loop and its assessment, using the system code TRACE (TRAC/RELAP Advanced Computational Engine). The model includes the main components of the loop, for some of which new methodologies were developed. The accuracy and reliability of the model were then evaluated by comparing simulation results with the experimental data obtained during the commissioning phase in October 2024, providing valuable insights for the further development of Energy Well.

2. Code Description

The code used for modeling the experimental Energy Well loop is TRAC/RELAP Advanced Computational Engine (TRACE, formerly called TRAC-M), version 5 patch 8 [12].

TRACE is an advanced, best-estimate reactor systems code developed by the U.S. Nuclear Regulatory Commission (NRC) as the result of a systematic effort to integrate four main systems codes (TRAC-P, TRAC-B, RELAP5 and RAMONA) together into one modernized computational tool. Analyses performed with this tool can be used as the basis for decisions concerning plant design, operation and safety. It is mainly used to simulate and analyze the neutronic–thermohydraulic behavior of light water reactors (LWRs), both pressurized water reactors (PWRs) and boiling water reactors (BWRs), under steady state, transient and accident conditions [12].

TRACE adopts a component-based approach to modeling a reactor system. Each physical part of a flow loop can be represented as a specific type of component, and each component can be further nodalized into several physical volumes (also called cells). These components include pipes (PIPE), vessels (VESSEL), pumps (PUMP), valves (VALVE), heat structures (HTSTR), power components (POWER), fills (FILL), breaks (BREAK) and others [12].

Within these components, it is possible to simulate a range of working fluids, including water; heavy water; helium; sodium; lead bismuth; lead; nitrogen; air; and molten salts such as FLiBe, FLiNaK, $KFZrF_4$ and $NaFZrF_4$. Customized fluids can also be imported through an External Property Table [12,13].

Another notable feature of TRACE is its control system, which consists of four basic elements: signal variables, control blocks, trips and component-action tables. These basic logic elements can be combined to simulate more complex systems, allowing for the modeling of the electronic and mechanical control systems of nuclear reactors, as well as accident scenarios [12].

3. Models and Methodology

The main components of the experimental facility are as follows:

- Main heater;
- Heat exchanger;
- Process vessel;
- Filling vessel;
- Pump;
- Bypass valve;
- Pipelines.

Thermocouples are placed at key points along the loop for temperature monitoring.

Regarding the TRACE model, whose final version is shown in Figure 1, not all the main components are included. The filling vessel and the bypass section of the loop are not modeled, for reasons described in the following paragraphs.

All pipelines are modeled with PIPE components, with an average diameter of around 21 mm, aiming to represent them as accurately as possible given the lack of three-dimensional modeling. Each PIPE component is associated with an HTSTR component to represent the solid wall, mainly composed of INCONEL 625 and insulation layers. Most components are made of INCONEL 625, except for the graphite block of the main heater. All of these components are covered with two layers of insulation: a 100 mm Fiberfrax Durablanket layer and an 80 mm Isover LSP layer. None of these materials is included in the TRACE database, so they were introduced as “User Defined Materials”.

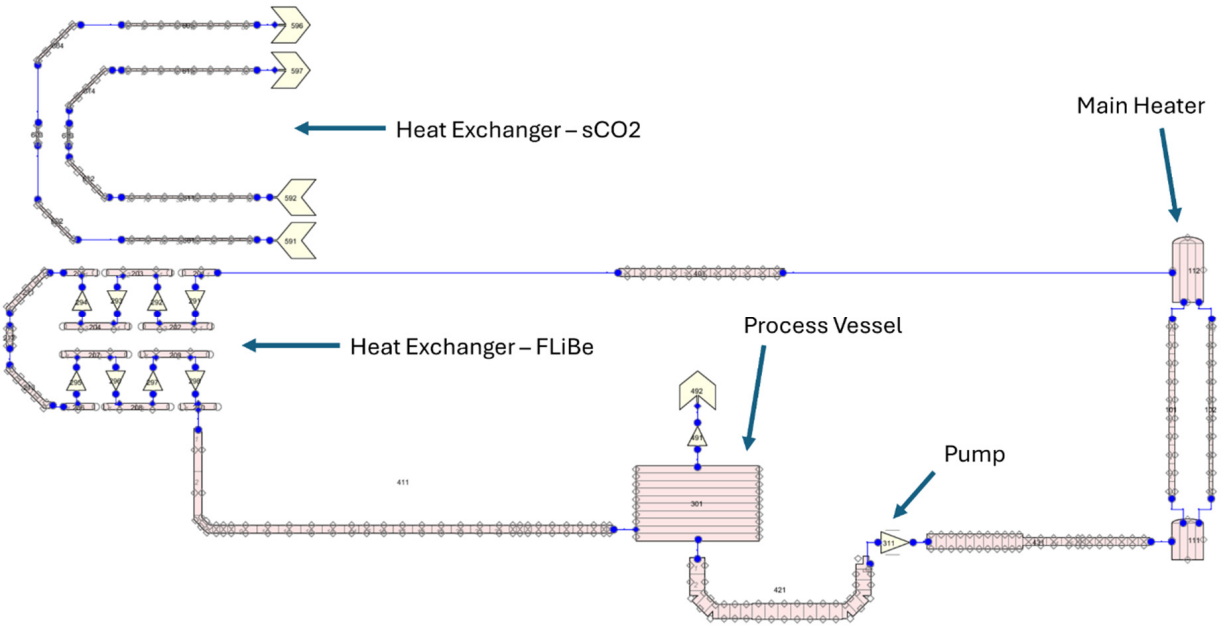

Figure 1. TRACE model of the EW experimental loop.

It is also important to describe the loop environment's external conditions, which are used as boundary conditions wherever a heat structure interfaces with the surroundings:

- Sink temperature = 293.15 K;
- Heat-transfer coefficient = 4.0 W/m^{2}K.

3.1. Main Heater

The main heater heats up the system through the Joule effect, simulating a segment of EW fuel. It is divided into three sections, inlet zone, core and outlet zone, all enclosed in a thin INCONEL 625 shell.

The core, 500 mm long, consists of five graphite blocks. Its cross-section, shown in Figure 2, has a diameter of around 108 mm and contains several channels of different sizes and purposes:

- A central channel through which FLiBe flows (d = 16 mm);
- A small channel designated for thermocouple placement (d $\simeq$ 7 mm);
- Six channels, called heating rods, each containing a central graphite rod, surrounded by a layer of INCONEL 625, with the electrical heaters located inside the graphite (d $\simeq$ 18 mm);
- Twelve channels: Six larger channels identical in size and purpose to the heating rods described above, and six smaller channels (d = 10 mm) through which the FLiBe flows;
- Two additional small channels for thermocouples.

Due to its complex cross-section, the modeling of the main heater required us to adapt a specific methodology previously developed [14]. This methodology is based on the principle of volume conservation to represent an equivalent section that can be easily modeled in the code.

The core is divided into two parts, as shown in Figure 2, each represented by a PIPE component. The central circle has a diameter of around 67 mm and includes the central FLiBe channel, six heating rods and one thermocouple channel. The development of the equivalent cross-section begins with the central FLiBe channel, which retains its original dimensions. The first layer surrounding the fluid is made of graphite, encompassing all graphite within a circle passing through the centers of the heating rods. Next, there are two

layers representing the material of the heating rods: an INCONEL 625 layer, including the thermocouple channel, and a layer for the heated graphite. Finally, an outer graphite layer represents the remaining matrix material. The result is shown in Figure 3.

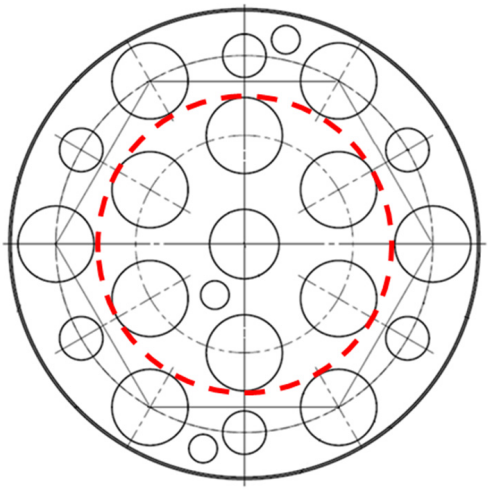

Figure 2. Main heater core cross-section.

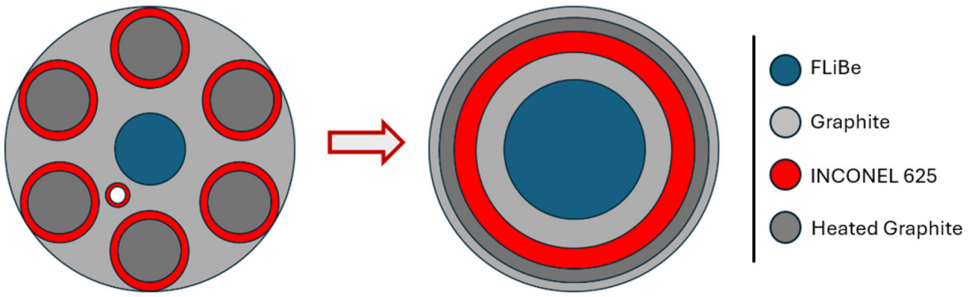

Figure 3. Development of the equivalent main heater cross-section.

In TRACE, this setup is represented by a vertical PIPE component for the FLiBe, coupled with a cylindrical HTSTR component representing all the solid material. The thicknesses of the equivalent section layers are calculated using Equation (1):

$$s_n = \sqrt{\frac{A_{FLiBe} + \sum_{j=1}^{n} A_j}{\pi}} - r_{FLiBe} - \sum_{j=1}^{n-1} s_j, \quad (1)$$

where

- s_n is the calculated thickness of the layer;
- A_{FLiBe} is the cross-sectional area occupied by FLiBe;
- $\sum_{j=1}^{n} A_j$ is the sum of the areas occupied by all materials within the calculated layer, excluding FLiBe;
- r_{FLiBe} is the radius of the FLiBe channel;
- $\sum_{j=1}^{n-1} s_j$ is the sum of the thicknesses of the material layers within the calculated layer, excluding the thickness of the layer calculated and the radius of the FLiBe channel.

This HTSTR component exchanges heat only internally with the FLiBe. No external boundary condition is applied.

For the second part of the cross-section, the outer ring, the same procedure is applied. Only 1/6 of the ring is simulated, and the HTSTR component includes 1/6 of the solid material, with a multiplicity factor of 6. Three additional layers are added: an INCONEL

625 layer accounting for the main heater shell, and two insulation layers. This HTSTR component transfers heat externally to the environment.

Lastly, the power generation must be modeled. To achieve this, the POWER component is used, allowing a power input value to be distributed within the assigned HTSTR component. As the input power is evenly distributed across the 12 heating rods, two POWER components are used, each assigned half of the total power, applied to the graphite layers associated with the heating rods.

The inlet zone is 102 mm long and serves as a coolant flow distributor, while in the outlet zone, 164 mm long, the flow mixes before entering the heat exchanger. In these regions, the flow is disrupted by structural elements and instrumentation.

The inlet zone is best represented by a VESSEL component, which allows for flow distribution by defining specific flow areas. It consists of one axial level and azimuthal sector, and two radial rings used to distribute the flow between the two core PIPE components. Following the same approach used for the core section, a HTSTR component is assigned to it.

The outlet zone is modeled in the same way.

3.2. Heat Exchanger

The heat exchanger is a "shell-and-tube" type with a horizontal U-shape, in which the sCO_2 flows inside the tubes while the FLiBe flows externally. The FLiBe enters from the top and exits from the bottom, flowing through free volume and encountering baffles. These obstacles, arranged in groups of four within the straight section, enhance heat transfer. On the other hand, the sCO_2 flows almost undisrupted inside 19 small tubes, moving from the bottom to the top, allowing for counterflow operation. A CAD drawing of a section of the heat exchanger is shown in Figure 4: the yellow and black lines represent, respectively, the approximate path of FLiBe and sCO_2, while the red lines represent the baffles.

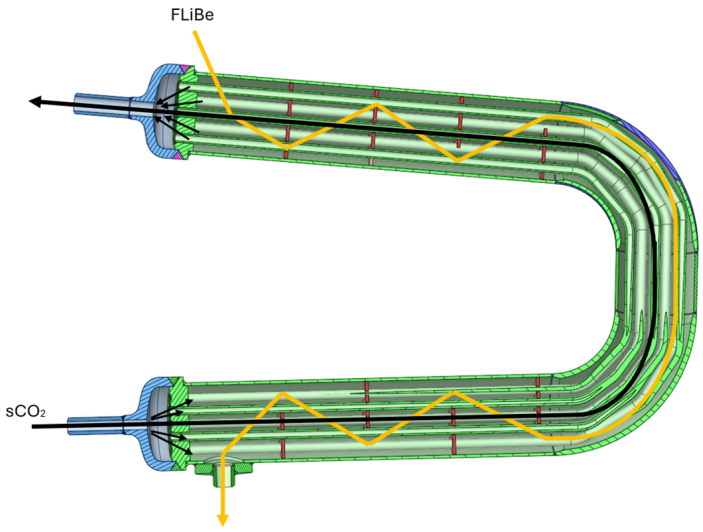

Figure 4. Heat exchanger section, CAD drawing.

The heat exchanger, enclosed in a thin INCONEL 625 shell, has a diameter of around 83 mm, while the sCO_2 tube's diameter is 7 mm. The total length is about 1150 mm.

This geometry cannot be directly represented in TRACE, primarily due to the internal tubes and the FLiBe pathway, which includes obstacles. Therefore, a new modeling methodology was developed, incorporating several simplifications necessitated by the lack of 3D modeling capabilities in TRACE.

The heat exchanger model is divided into two parts: the FLiBe side, connected to the loop, and the supercritical CO_2 side, which remains hydraulically disconnected from the rest of the loop, as shown in Figure 1.

On the FLiBe side, the goal was to simulate the serpentine motion caused by the baffles, as well as the directional changes imposed by the U-shaped structure. Consequently, it is divided into two parts: the straight sections, which contain baffles, and the central section, which is mostly curved and baffle-free.

In the model, the straight sections consist of multiple PIPE components connected in such a way as to reproduce the serpentine flow motion. As shown in Figure 5, this approach involves horizontally dividing the section in half, so that each half includes two baffles. Then, for each space between two baffles, or between the section inlet/outlet and a baffle, a PIPE component is defined. The dimensions of the PIPE components are equal to the volume occupied by FLiBe in that section. The connection between the upper and lower halves is made laterally by pairing cells, where each cell in the upper half connects to its corresponding cell in the lower half using single-junction components.

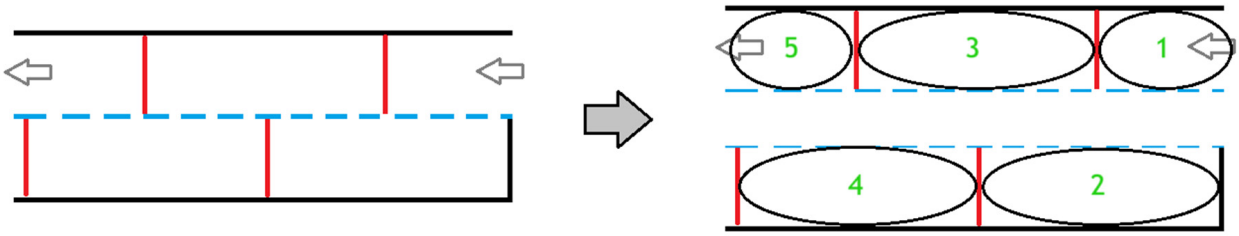

Figure 5. Development of the heat exchanger's methodology.

In the central, curved section, the salt flow aligns with the shape of the heat exchanger. Three PIPE components are defined for this section, simulating the change in flow direction.

Each PIPE component is coupled with an HTSTR component, representing the shell and insulation layers of the heat exchanger. These components exchange heat internally with the FLiBe and externally with the surrounding environment.

The supercritical CO_2 circuit was not entirely modeled in TRACE. Only the part inside the heat exchanger is represented, as shown in Figure 1. In the model, the 19 internal tubes are simulated in two independent PIPE components. A FILL and a BREAK component are modeled for each of these PIPE components to simulate inlet and outlet. HTSTR components are assigned to each PIPE component, with a thickness equal to a single tube. These HTSTR components allow for heat transfer between the FLiBe and the sCO_2 sides. The two sCO_2 PIPE components are coupled to the internal and external FLiBe side by specific HTSTR component settings.

Following the commissioning of the experimental loop and the first simulations, a defect in the heat exchanger was identified. Given its configuration, not all the available volume fills with FLiBe. A portion of it remains occupied by nitrogen, which fills the whole loop during non-operational phases. To represent the effect of reduced heat-transfer efficiency, a thin layer of nitrogen is added within the INCONEL 625 in the HTSRT component, achieving the same thermal exchange as observed in the experimental loop.

Regarding the fluid, nitrogen was selected as a substitute for sCO_2 because it most closely matches its thermophysical properties among the built-in TRACE fluids. Additionally, since the focus is on the FLiBe side, we decided to modify the pressure in the secondary circuit to further align the properties of nitrogen with those of sCO_2. As shown in Table 1, the optimal pressure value is 25 MPa, which replaces the operational pressure of the sCO_2 side. Engineering Equation Solver (EES) V9.994-3D [15] software was used to calculate carbon dioxide and nitrogen properties, using as reference temperature the average

temperature along the sCO_2 tubes. This approach is acceptable because the computational domain on the sCO_2 side is very small, leading to only minor variations in thermophysical properties within the domain. Moreover, the heat exchanger considered in the model operates on the sCO_2 side far from the critical point, where changes in thermodynamic properties are no longer abrupt or pronounced.

Table 1. Properties comparison, CO_2 and N_2.

	Cp [kJ/kgK]	Density [kg/m^3]	Thermal Conductivity [W/mK]	Viscosity [kg/ms]
CO_2 (15 MPa)	1.217	100.1	0.05836	3.551×10^{-5}
N_2 (15 MPa)	1.140	61.12	0.05696	3.605×10^{-5}
(delta)	(0.077)	(39)	(0.0014)	(-5.4×10^{-7})
N_2 (25 MPa)	1.152	97.90	0.05896	3.680×10^{-5}
(delta)	(0.065)	(2.2)	(−0.00060)	(-1.3×10^{-6})

In theory, it would be possible to add a fluid, like carbon dioxide, via an External Property Table (XPTB), following the procedure detailed in [16]. However, at the time of the study, an unknown error consistently occurred when attempting to generate the table, thus requiring the use of surrogate fluid.

3.3. Process Vessel

The process vessel serves as an expansion volume and a storage tank during the normal operation of the loop. It collects the fluid coming from the heat exchanger and the bypass section, while directing it to the pump. The FLiBe occupies around 40% of the volume available, while the rest is filled with nitrogen gas, which prevents corrosion and protects pressure sensors. It has a height of 200 mm and an internal diameter of 344 mm.

In TRACE, this component is modeled simply as a vertical PIPE component with the dimensions of the process vessel. Furthermore, the non-condensable gas option must be enabled so that N_2 is represented in the upper cells of the PIPE component. HTSTR components are assigned to the vessel, exchanging heat with the fluids internally and with the environment externally.

A BREAK component is also connected to the top of the process vessel, imposing the pressure boundary condition for the loop.

The process vessel inlet is placed at the bottom instead of at the top, where it should be located. With the inlet at the top, the software simulates FLiBe falling downward, passing through multiple control volumes occupied by nitrogen. This causes substantial computational issues, because TRACE is not optimized for this type of configuration, particularly when molten salt is used as the primary fluid. Placing the inlet close to the bottom allows the incoming FLiBe to flow directly into the FLiBe zone, thereby streamlining the simulation without affecting the results of primary interest.

In addition to the process vessel, the facility also includes a filling vessel. However, this component is not part of the model. Serving as a collection tank during non-operational phases, its presence in the model would be unnecessary, since the simulations exclude startup and transient conditions. For the same reason the process vessel internal heating is not modeled either.

3.4. Pump

The hydrodynamic pump, designed and built by CVŘ, circulates FLiBe through the loop. Although the pump is physically small, it remains "oversized" compared to the actual flow requirements of the loop. Due to this, 90% of the flow is redirected via a bypass

valve to the process vessel. Unfortunately, essential input data for the TRACE model, such as curves linking torque and power to rotational speed, are unavailable. For this reason, a highly simplified pump model has been adopted, serving as a boundary condition that imposes a constant flow rate. As a result, the bypass section, including pipes and valve, is not modeled.

3.5. Pressure Losses

The resistance to flow across various piping components, such as fittings, valves and connections, significantly contributes to the pressure drop within the overall piping system. Since a universally standardized methodology does not exist for calculating pressure losses, this section briefly examines the methodology employed to calculate the friction factor (k) for localized head losses along the loop, an essential input for TRACE when determining total pressure losses [17].

Regarding the localized head losses related to changes in cross-section, the Hooper Method [18] was selected, as it accounts for a wide range of Reynolds numbers. Equations for loss coefficients vary based on the contraction/enlargement angle (ϑ) and Reynolds number, as well as being a function of the diameter ratio and Darcy factor. For abrupt sectional changes ($\vartheta = 180°$), simplified equations are used.

For head losses associated with changes in flow direction, the Darby Method [19] was applied. This method, commonly used for sharp bends or tees, accounts for fitting dimensions and types and provides reliable results even in laminar flow conditions. The friction factor is determined using a specific formula with tabulated constants for different components.

Lastly, for complex geometries such as the heat exchanger or main heater, where the above correlations cannot be directly applied, predefined k-factors are assigned:

- Changes in cross-section = 0.5;
- Changes in direction = 0.25.

These values are also used to simulate the flow disruption in the main heater's inlet and outlet zones.

The applied correlations are consistent with the theory of thermohydraulic similarity and are valid within the appropriate range of Reynolds and Prandtl numbers. However, it is important to mention that these correlations are water-based and therefore may not perfectly represent the FLiBe behavior. They are also generally more accurate for turbulent or high-speed flows. The calculation of head losses for laminar flow is more complex, and this may lead to increased uncertainty in the results.

4. Experimental Campaign

During 2024, the EW experimental facility (including the loop) was used to perform two experimental campaigns [20]. The main objectives of these campaigns were to assess the operational regimes, including the heat transfer from the FLiBe to sCO_2; to characterize individual component performance; and to generate high-quality data for model validation and system design.

The first campaign, led in March 2024, served as a commissioning phase. It focused on assessing the key components, such as the FLiBe pump, electrical heaters and control system, as well as on developing reliable start-up and shut-down procedures.

Then, in October 2024, the second campaign was performed. The objectives were to demonstrate facility capability to be started and operated repeatedly for extended periods, to investigate the coupled behavior of the FLiBe and sCO_2 circuits, and to obtain steady-state data for model assessment.

The second commissioning of the loop started with preheating the entire facility to the target temperature. This procedure lasted about two days, in which the maximum temperature gradient was maintained at 50 K/h to avoid thermal stress. During this period, several stepwise holds at intermediate temperatures were made to ensure safe melting and homogenization of the salt in order to prevent the deterioration of the components' performances.

Once the system temperature exceeded the salt melting point (732 K), the pump was tested for free rotation and then started. The molten salt was displaced from the filling vessel into the circuit using pressurized nitrogen, while the stability of the mass flow was monitored indirectly via pressure signals and pump discharge conditions. When stable flow conditions were reached, the sCO_2 loop was activated and synchronized with the FLiBe loop, enabling heat transfer across the heat exchanger.

During the operation, several boundary conditions were periodically modified to assess the system's response. On the FLiBe side, the pump's rotational speed, the electrical heaters' power and the pipe's heating levels were varied. On the sCO_2 side, both the mass flow rate and the inlet temperature at the heat exchanger were modified.

Also, tests were performed both with auxiliary pipe heating on and off. The latter configuration was used to represent and verify the self-sustaining operation conditions, which are more representative of the EW system's behavior.

This longer campaign allowed for the acquisition of relevant experimental data, which were analyzed by identifying steady-state intervals, referred to as cases.

A case is defined as a period of time in which the main parameters are stable under steady-state condition, except for small oscillations due to the perturbation of the flow that are normally below the measurements' uncertainty. Out of all the cases, we decided to analyze only those in which the auxiliary heating system was switched off. These cases are more relevant because the system self-maintains its operating temperatures, without extra heating, similar to the Energy Well steady state. For this reason, Cases 6 and 8 were selected. Case 6 is used to provide an initial assessment of the model, which reached its final form after several simulations under these conditions, in a calibration phase. Case 8 is used to assess the model performance and identify its limitations and potential areas of improvement.

Table 2 shows all the relevant values related to Cases 6 and 8. The highlighted values are those used as input values, while the others are used to benchmark the model. The latter are represented by the orange line in Figures 6–14.

T17 is the thermocouple that measures the FLiBe temperature directly in the flow, before entering the main heater. TC11 and TC12 are instead placed on the pipe surface, respectively, at the main heater outlet and heat exchanger outlet. The pressure in the FLiBe loop is provided only for Case 6, but it is used for both cases during simulations as a boundary condition at the process vessel BREAK component.

It is important to mention that these values are subject to measurement uncertainties. For the thermocouples, the range of uncertainty given is equal to 0.4% of the measured value $\pm$ 0.5 K. The figures of the following section present this uncertainty with a yellow band. Additionally, their exact location is unknown, further increasing the uncertainty of the measurements. The mass flow rate is also affected by uncertainties, since it is calculated using energy balances on the loop components, as no specific instrumentation was available.

Table 2. Main data from the experimental campaign.

	FLiBe Side	
	Case 6	**Case 8**
Power [W]	**6844.0**	**6844.0**
T17 [K]	822.94	823.57
TC11 [K]	829.65	827.19
TC12 [K]	814.69	819.05
p [MPa]	**0.14370**	**-**
dp [MPa]	0.010700	0.011900
***ṁ* [kg/s]**	**0.58600**	**1.1410**
HTC [W/m^{2}K]	1115.0	1371.0
	sCO_2 Side	
	Case 6	**Case 8**
T_{in} [K]	**751.49**	**751.79**
T_{out} [K]	805.98	809.73
p [MPa]	**14.000**	**14.000**
***ṁ* [kg/s]**	**0.090000**	**0.090000**

5. Results

The simulations are run as null transient for 20,000 s to ensure that the proper stable conditions are reached. Before each simulation, boundary conditions and initial values are set according to each case, including pressure losses.

Due to its importance, the first parameter that has been checked is the temperature at the main heater inlet, shown in Figures 6 and 7. The N_2 layer thickness in the heat exchanger's HTSTR components was modified in order to reach a temperature at the main heater inlet, matching Case 6. The value reached is equal to 823.24 K, which is close to the experimental value and within the range of uncertainty. For Case 8, the result is 824.38 K, which is consistent as well. However, for this case, the model was not further adjusted.

Regarding the main heater outlet temperature, shown in Figures 8 and 9, the simulation results are lower than the reference data. For Case 6, the simulation result is 826.88 K, and for Case 8, it is 826.20 K. Despite the difference, these results are within the thermocouple uncertainty range and therefore consistent.

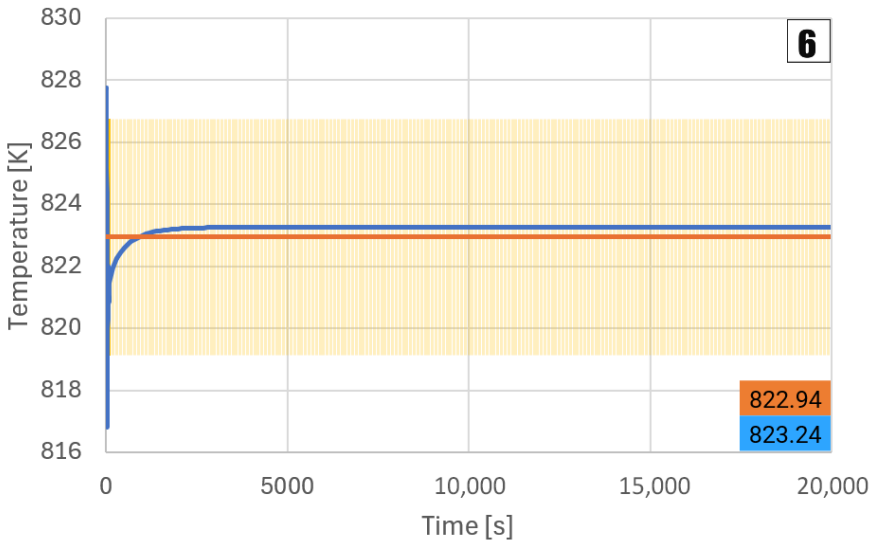

Figure 6. Temperature T17, main heater inlet, Case 6.

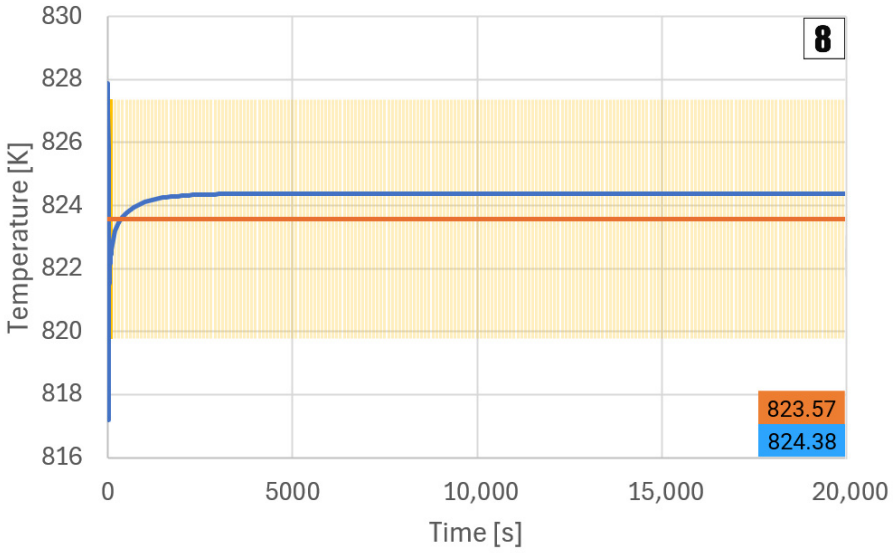

Figure 7. Temperature T17, main heater inlet, Case 8.

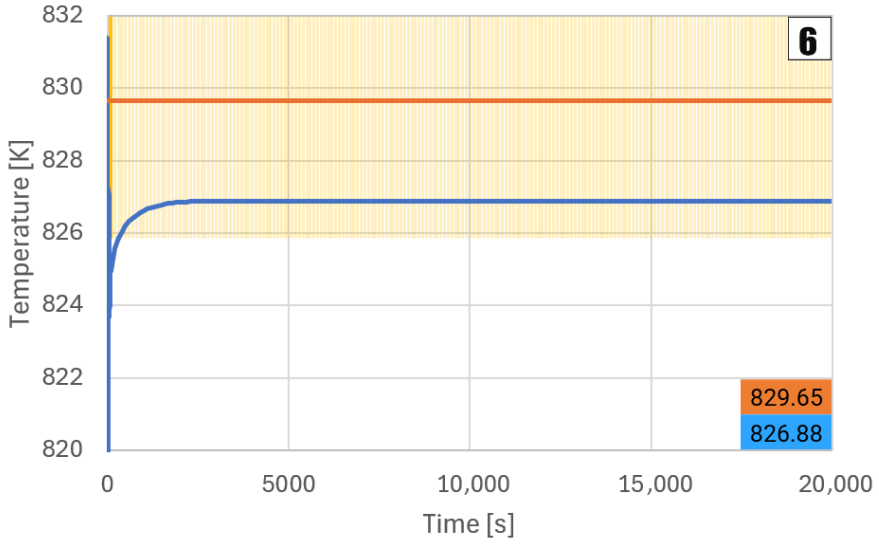

Figure 8. Temperature TC11, main heater outlet, Case 6.

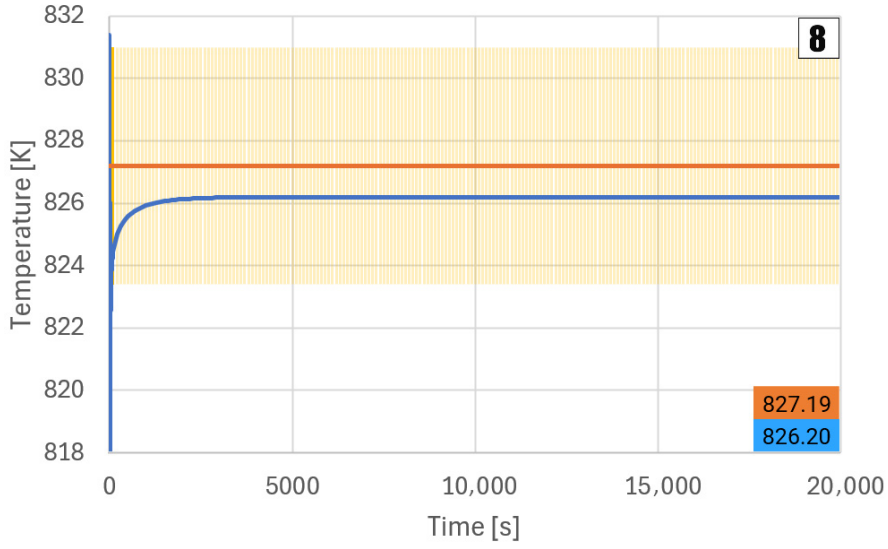

Figure 9. Temperature TC11, main heater outlet, Case 8.

The main heater thermocouples, located in the graphitic core, are also checked in the simulations: three for both PIPE components, in the same axial location as in the real component. As underlined in the Case 6 results, shown in Figure 10, the model cannot precisely represent the graphite temperature profile during operation. The temperatures and their variation on the axial level are different and inconsistent with the experiment in both the cases analyzed. This could be related to a different heat removal efficiency depending on the channel, different flow distribution in the model or inaccuracy of the graphite properties, which were provided only for room temperature. It should be noted that the TRACE model is based on a one-dimensional representation of a complex system, where certain physical phenomena are necessarily simplified. For this, selected sensitivity analyses were conducted as part of the work described in [21]. However, the resulted discrepancies do not affect the measured outlet temperature of the salt.

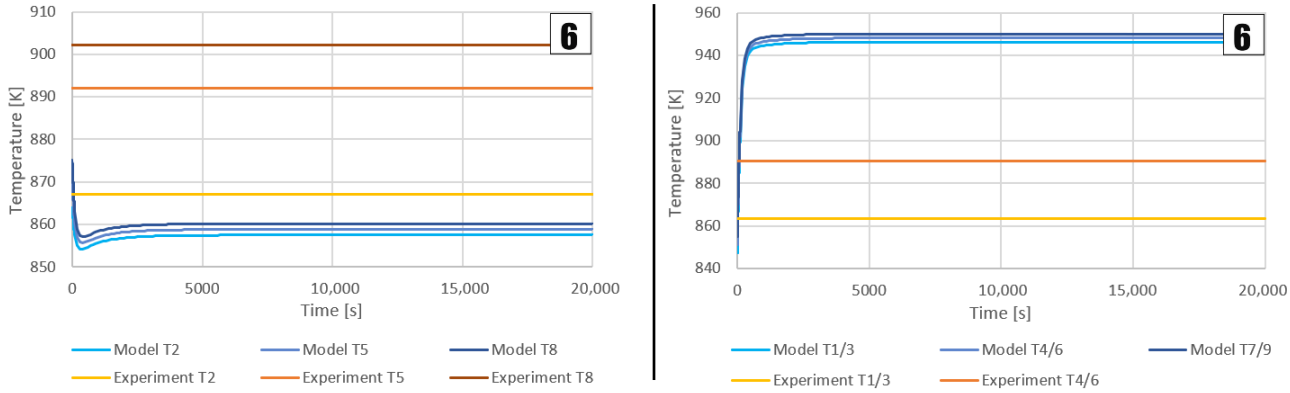

Figure 10. Main heater's graphite temperature, Case 6: central part on the left, and outer part on the right.

For the heat exchanger, the model shows limited heat losses between the two components (about 0.03 K). Figures 11 and 12 show the outlet temperature on the FLiBe side. It is notable that in the experimental loop, the FLiBe releases more heat to the sCO_2 than in the model. Even though the temperature difference is 8 K for Case 6, and 5 K for case 8, the results are consistent. In fact, in the experimental loop, there are some heating phenomena (such as thermal inertia phenomena, pump heating through compression and electrical heating in the bypass section) which are not represented in the model. Due to this, it is reasonable that the temperature at the heat exchanger outlet is close to that at the main heater inlet, as heat losses are limited.

Figures 13 and 14 show the N_2 outlet temperature in the heat exchanger. For Case 8, the difference between model and experiment is smaller than for Case 6, and the model value is within the uncertainty range. In the experiment, there is higher heat transfer to the secondary loop, which causes the outlet flow to be hotter. In the model, this does not occur because the input power must be matched by the heat transferred outside through the heat exchanger and heat losses. Considering also all the simplifications involved (surrogate fluid, open loop, etc.), the results can be considered consistent.

The differential pressure caused by the introduced pressure losses was analyzed as well. Figures 15 and 16 display different pressure values in the model:

- Pressure at the process vessel (boundary condition);
- Pressure measured at the pump discharge;
- Pressure measured at the pump discharge with no k-factors applied.

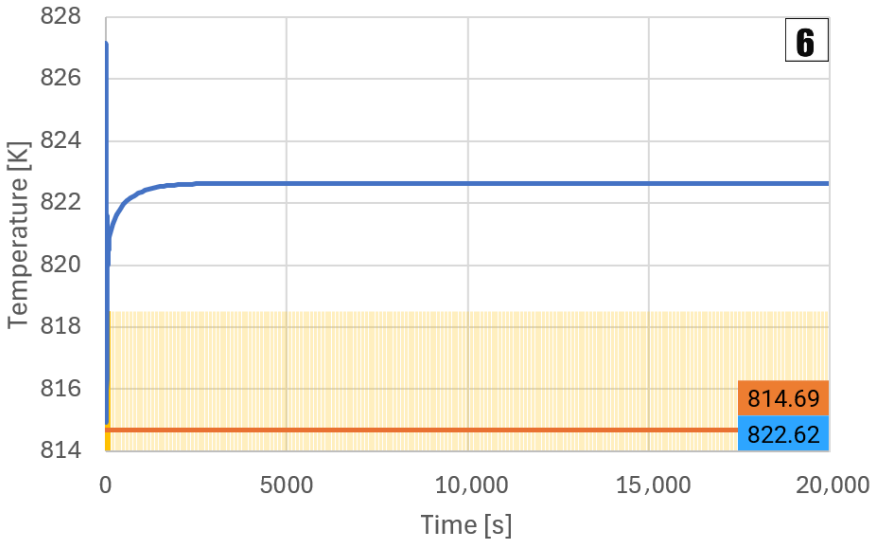

Figure 11. Temperature TC12, heat exchanger's FLiBe outlet, Case 6.

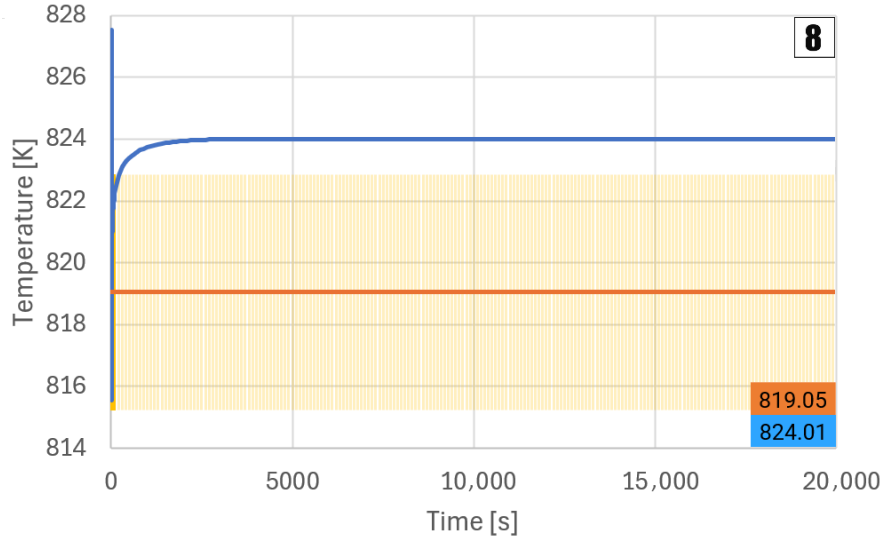

Figure 12. Temperature TC12, heat exchanger's FLiBe outlet, Case 8.

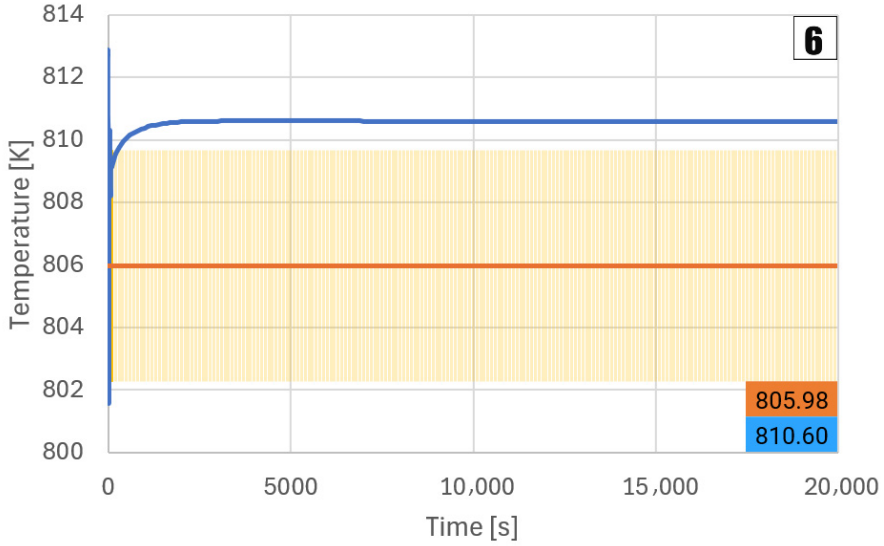

Figure 13. Temperature tout, heat exchanger's sCO_2 outlet, Case 6.

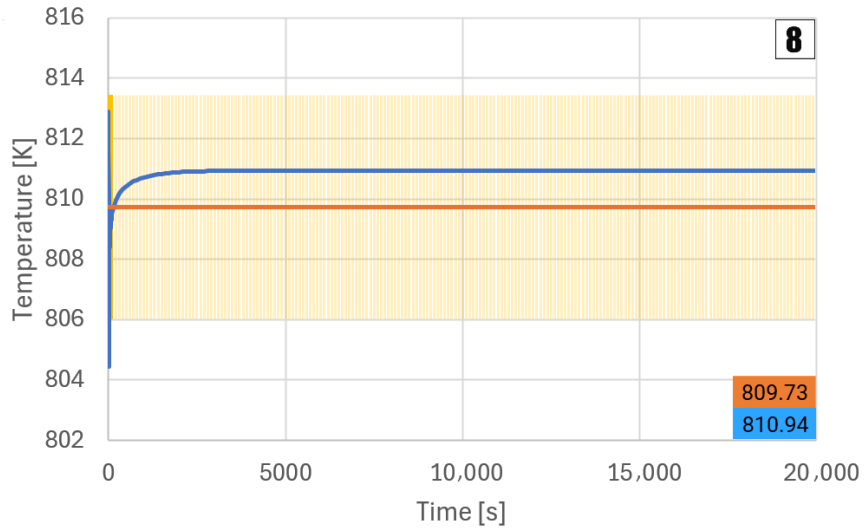

Figure 14. Temperature tout, heat exchanger's sCO_2 outlet, Case 8.

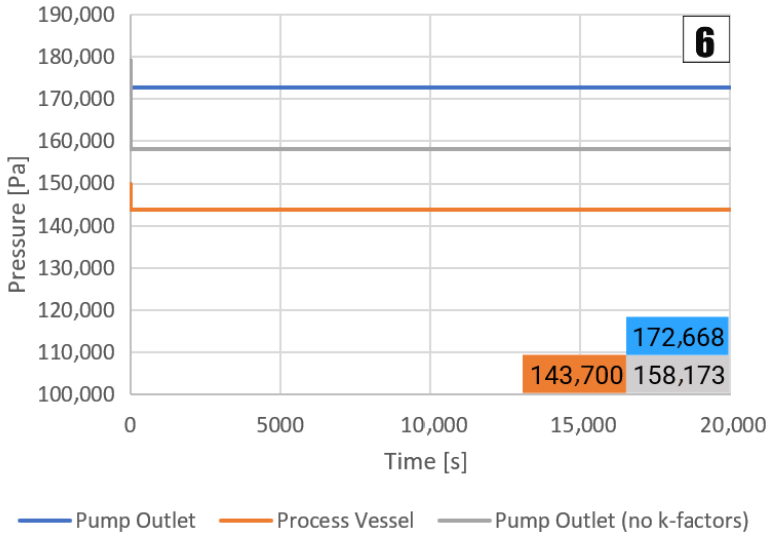

Figure 15. Pressures in the model, Case 6.

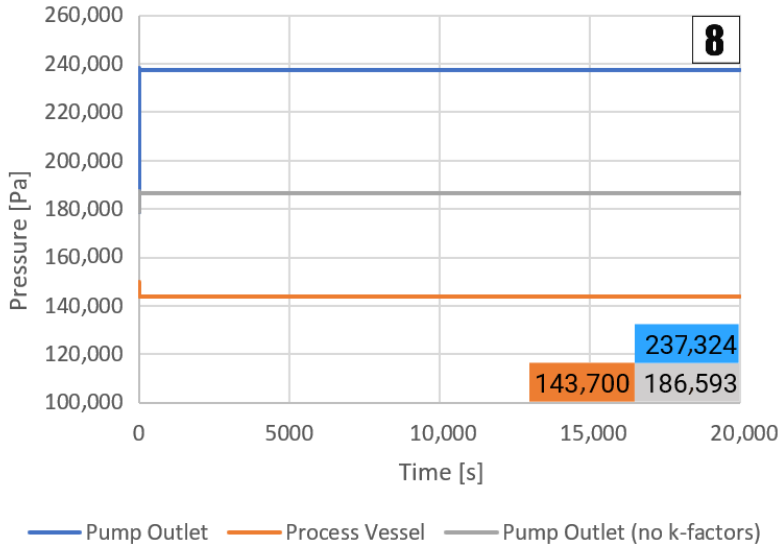

Figure 16. Pressures in the model, Case 8.

The pressure difference between process vessel and pump (respectively, blue and orange lines) represents the total pressure differential. However, the value presented in Table 2 differs. It does not include the "dead" pressure difference between the sensors. A simulation was performed without assigning k-factors to the model, resulting in the grey line. The difference between the two pump measurements correspond to the experimental pressure differential. For Case 6, this value is equal to 14,495 Pa, which is consistent compared to the experimental 10,700 Pa, taking into account the pressure loss correlations and simplifications adopted.

In Case 8, the pump pressure measurements show higher values, as expected. The increase in mass flow rate results in higher hydrostatic pressure. However, while in the experiment the pressure differential is similar between the two cases, for Case 8, it is 50,731 Pa, more than four times the experimental one. A reason for this large discrepancy between experiment and model likely lies in the change in correlation equations, due to different flow conditions, since they are a function of the Reynolds number, which is higher in Case 8. Using alternative correlations might produce results more consistent with the experiment. This could be a topic for future studies. It is also important to note that pressure measurements in molten salt circuits are generally complicated, resulting in increased measurement uncertainties. In the present case, the pressure measurement was addressed by maintaining a gas cushion between the molten salt level in the sampling line and the sensor in order to eliminate the risk of salt freezing in the sampling tube. Consequently, the measurement uncertainty is significantly increased by the gas behavior within the sampling tube, and the measured values cannot be directly used for benchmarking the circuit pressure losses.

During the simulations, instabilities were also found in the process vessel. These instabilities are linked to the interaction of the non-condensable gas with a non-standard fluid, in this case, FLiBe. The instability of this interaction was also observed with lead in [22]. However, this phenomenon has no significant influence on the analysis results.

Finally, as part of the project activity, the heat-transfer coefficients (HTCs) were estimated for comparison with experimental data and the literature values. Unfortunately, due to the experimental limitations and uncertainties mentioned above, it is not possible to determine the HTCs in the heat exchanger with sufficient accuracy. However, data from the main heater, which is sufficiently instrumented, can be used.

For the TRACE model, an average of the axial HTC values was calculated for the two PIPE components. Then, a weighted average based on the flow areas was computed. The result is 1041.9 W/m^2K for Case 6 and 1335.7 W/m^2K for Case 8; these results are consistent with the experimental data in Table 2. For further comparison, the HTC was also determined analytically using the Hausen correlation, detailed in [23]. From this, the HTC is 536 W/m^2K for 10 mm diameter channels and 368 W/m^2K for the 16 mm diameter central channel, approximately half of the previous results. The difference may be due to measurement uncertainty or inaccuracy. Another source of deviation may be the uneven power distribution caused by possible uneven flow distribution in individual channels, which cannot be evaluated from the data. However, the obtained results are consistent with those reported in [24], where experimentally evaluated heat transfers in laminar flow were also higher than the results from correlations in the literature. It should also be mentioned that fully developed laminar flow cannot be assumed in the heater, as the heater is located directly behind a 90° elbow and other circuit components. This may also lead to higher values than those given by correlations assuming fully developed laminar flow.

All the main experimental and model results are summarized and compared in Table 3.

Table 3. Comparison between experimental data and model predictions.

	Case 6 Experiment	**TRACE**
T17 [K]	822.94	823.24
TC11 [K]	829.65	826.88
TC12 [K]	814.69	822.62
T_{out_sCO2} [K]	805.98	810.60
dp [MPa]	0.010700	0.014495
HTC [W/m^{2}K]	1115.0	1041.9
	Case 8 Experiment	**TRACE**
T17 [K]	823.57	824.38
TC11 [K]	827.19	826.20
TC12 [K]	819.05	824.01
T_{out_sCO2} [K]	809.73	810.94
dp [MPa]	0.011900	0.050731
HTC [W/m^{2}K]	1371.0	1335.7

6. Discussions and Conclusions

The simulations based on the commissioning experimental data revealed several important insights. Overall, the model was consistent, particularly with respect to the heat exchanger and the general performance of the main heater. However, some discrepancies were observed, notably within the main heater's active channel. These inconsistencies pointed to potential areas for improvement, such as refining the simulation methodology or reassessing the properties of materials. The model also uncovered phenomena of broader relevance. For instance, issues with incorporating an external property table for CO_2 were identified and subsequently reported to the USNRC. Additional limitations were observed, such as those associated with non-condensable gas instabilities. Furthermore, these simulations have proven to be an essential tool for collaboration with technicians working on the experimental loop, enabling the identification of inconsistencies in certain sensors measurements and supporting their resolution. This work provides a strong foundation for future improvements.

A key next step will involve introducing CO_2 as the secondary fluid in the heat exchanger, thereby enabling a more detailed investigation of convection involving supercritical CO_2 [25], particularly its interaction with FLiBe.

Beyond these technical enhancements, the project opens opportunities for international collaboration, promoting shared progress in the development of molten salt reactor technologies, as well as other SMR projects that share similar features and goals, like KRONOS MMR [26], designed and developed by NANO Nuclear Energy Inc., or R&D activities carried out in academia and research centers [27]. Thanks to its dedicated facility, it also plays a crucial role in advancing knowledge, as it provides unique data and expertise at a time when suitable infrastructures for the study of molten salts and laminar flows are still very limited. Moreover, the facility offers the potential to conduct experiments over a broader range of operating conditions to derive new correlations for both heat transfer and pressure losses in FLiBe-type salts.

This work underscores the potential of TRACE as a powerful tool for modeling and simulation in this field, encouraging broader use of the code within the global research community. It also will push forward several activities and possible new projects. In particular, as said before, the work can continue to enhance TRACE by improving the know-how of heat transfer and flow regime characterization for molten salts and sCO_2.

The understanding of these phenomena will lead to the improvement of the EW design, with several crosscutting in advanced SMRs, both primary and secondary circuits, and fusion technologies. Moreover, it will expect to continue in several projects in domestic domains, such as TAČR, and international domains, such as IAEA CRP, EUROfusion and EURATOM.

Author Contributions: Methodology, G.L. (Giacomo Longhi) and G.M.; validation, G.L. (Giacomo Longhi) and T.M.; formal analysis, G.L. (Giacomo Longhi) and G.M.; investigation, G.L. (Giacomo Longhi); resources, G.L. (Guglielmo Lomonaco) and G.M.; data curation, T.M.; writing—original draft preparation, G.L. (Giacomo Longhi); writing—review and editing, G.L. (Giacomo Longhi), G.L. (Guglielmo Lomonaco), T.M. and G.M.; supervision, G.L. (Guglielmo Lomonaco) and G.M.; project administration, G.M. All authors have read and agreed to the published version of the manuscript.

Funding: The presented work has been realized within Institutional Support by Ministry of Industry and Trade of the Czech Republic. Also, the presented results were obtained using the CICRR infrastructure, which is financially supported by the Ministry of Education, Youth and Sports—project LM2023041.

Data Availability Statement: The data presented in this study are not publicly available due to project-related limitations (unless already public and therefor part of the presented references). Data may be made available by the authors upon reasonable request.

Acknowledgments: The presented work was realized with institutional support from the Ministry of Industry and Trade of the Czech Republic. A special thanks to Antonio Dambrosio and Mathieu Reungoat for their valuable support throughout this work.

Conflicts of Interest: The authors declare no conflict of interest.

Abbreviations

The following abbreviations are used in this manuscript:

SMRs	Small modular reactors
MMRs	Micro modular reactors
CVŘ	Centrum Výzkumu Řez
EW	Energy Well
TRISO	Tri-Structural Isotopic
FLiBe	Fluoride Lithium Beryllium
CO_2	Carbon dioxide
sCO_2	Supercritical carbon dioxide
TRACE	TRAC/RELAP Advanced Computational Engine
TAČR	Technologická Agentura České Republiky
NRC	Nuclear Regulatory Commission
LWRs	Light water reactors
PWRs	Pressurized water reactors
BWRs	Boiling water reactors
HTSTR	Heat structure
CAD	Computer-Aided Design
EES	Engineering Equation Solver
XPTB	External Property Table
N_2	Nitrogen
HTC	Heat-transfer coefficient
USNRC	United States Nuclear Regulatory Commission
IAEA CRP	International Atomic Energy Agency Coordinated Research Project
EURATOM	European Atomic Energy Community

References

1. European Commission. The European Green Deal. Available online: https://commission.europa.eu/strategy-and-policy/priorities-2019-2024/story-von-der-leyen-commission/european-green-deal_en (accessed on 15 December 2025).
2. European Commission. Small Modular Reactors Explained. Available online: https://energy.ec.europa.eu/topics/nuclear-energy/small-modular-reactors/small-modular-reactors-explained_en#global-action-on-smrs (accessed on 15 December 2025).
3. World Nuclear News. Czech Republic Selects Rolls-Royce SMR for Small Reactors Project. Available online: https://www.world-nuclear-news.org/articles/czech-republic-selects-rolls-royce-smr-for-small-reactors-project (accessed on 15 December 2025).
4. Ruščák, M.; Melichar, T.; Syblík, J.; Frybort, O.; Harut, D.; Losa, E.; Mareček, M.; Mazzini, G.; Reungoat, M.; Pilát, J.; et al. Energy Well: Concept of 20 MW Microreactor Cooled by Molten Salts. *J. Nucl. Eng. Radiat. Sci.* **2021**, *7*, 021302. [CrossRef]
5. Lomonaco, G.; Mainardi, E.; Marková, T.; Mazzini, G. Approaching nuclear safety culture in fission and fusion technology. *Appl. Sci.* **2021**, *11*, 4511. [CrossRef]
6. Mazzini, G.; Benčík, M.; Reungoat, M. Thermohydraulic Simulation of Energy Well Micro Modular Reactor Using System Codes. In Proceedings of the 2024 31st International Conference on Nuclear Engineering, Prague, Czech Republic, 4–8 August 2024.
7. Gomes, D.d.S. Overview of the Physical Properties of Molten Salt Reactor Using Flibe. *J. Eng. Res.* **2023**, *3*, 2–12. [CrossRef]
8. Boussier, H.; Delpech, S.; Ghetta, V.; Heuer, D.; Holcomb, D.; Ignatiev, V.V.; Merle, E.; Serp, J. The molten salt reactor (MSR) in generation IV: Overview and perspectives. *Prog. Nucl. Energy* **2014**, *77*, 308–319. [CrossRef]
9. Jiang, D.; Zhang, D.; Li, X.; Wang, S.; Wang, C.; Hao, Q.; Guo, Y.; Tian, X.W.; Su, G.; Qiu, S.Z. Fluoride-salt-cooled high-temperature reactors: Review of historical milestones, research status, challenges, and outlook. *Renew. Sustain. Energy Rev.* **2022**, *161*, 112345. [CrossRef]
10. U.S. Department of Energy. TRISO Particles: The Most Robust Nuclear Fuel on Earth. Available online: https://www.energy.gov/ne/articles/triso-particles-most-robust-nuclear-fuel-earth (accessed on 15 December 2025).
11. Technology Agency of the Czech Republic. Technologická Agentura České Republiky. Project Number: TK02030125. Available online: https://tacr.gov.cz/en/ (accessed on 15 December 2025).
12. U.S. Nuclear Regulatory Commission. *TRACE V5.0 PATCH 8 USER'S MANUAL Volume 2: Modeling Guidelines*; U.S. Nuclear Regulatory Commission: Washington, DC, USA, 2022.
13. U.S. Nuclear Regulatory Commission. *TRACE V5.0 PATCH 8 USER'S MANUAL Volume 1: Input Specification*; U.S. Nuclear Regulatory Commission: Washington, DC, USA, 2023.
14. Wang, C.; Sun, K.; Hu, L.-W.; Zhang, D.; Tian, W.; Qiu, S.; Su, G.H. Transient safety analysis of a transportable fluoride-salt-cooled high-temperature reactor using RELAP5-3D. *Nucl. Technol.* **2017**, *198*, 1–16. [CrossRef]
15. F-Chart Software. Engineering Equation Solver (EES). Available online: https://fchartsoftware.com/ees/ (accessed on 15 December 2025).
16. Garrett, G. Comparison of Water, Helium, and Carbon Dioxide as Coolants for Next Generation Power Plants Using Trace. Master's Thesis, The Pennsylvania State University, State College, PA, USA, 2018.
17. Kilkovský, B.; Jegla, Z.; Stehlík, P. Comparison of Different Methods for Pressure Drop Calculation in 90° and 180° Elbows. *Chem. Eng. Trans.* **2011**, *25*, 243–248.
18. Hooper, W.B. Calculate Head Loss Caused by Change in Pipe Size. *Chem. Eng.* **1988**, *95*, 89–92.
19. Darby, R. Correlate Pressure Drops Through Fittings. *Chem. Eng.* **2001**, *108*, 127–130.
20. Kriz, D.; Melichar, T.; Filip, R.; Hasek, J. Coupling of Molten Salt and Supercritical CO_2 Circuits: Design and Operational Experience. In Proceedings of the 6th Edition of the European Conference on Supercritical CO_2(sCO_2) for Energy Systems, Delft, The Netherlands, 9–11 April 2025.
21. Čižek, T. CFD Simulation of a Heater in an Experimental Molten Salt Loop. Master thesis, Czech Technical University in Prague, Prague, Czech Republic, 24 June 2025.
22. Morresi, G. Cooling System Simulation for Lead Fast Reactor using TRACE. November 2024, Transmutex. Available online: https://www.nrccodes.com/CAMP/CAMP%20Minutes%20and%20Presentations/Forms/Default%20View.aspx?RootFolder=/CAMP/CAMP%20Minutes%20and%20Presentations/2024%2002%20-%20Fall%20(Rockville,%20MD,%20USA)/Presentations/03%20Technical%20Reports (accessed on 15 December 2025).
23. Incropera, F.P.; DeWitt, D.P.; Bergman, T.L.; Adrienne, L. *Fundamentals of Heat and Mass Transfer*, 6th ed.; John Wiley & Sons: Hoboken, NJ, USA, 2007.
24. Mehrabian, M.A.; Mansouri, S.H.; Sheikhzadeh, G.A. The Overall Heat Transfer Characteristics of a Double Pipe Heat Exchanger: Comparison of Experimental Data with Predictions of Standard Correlations. *IJE Trans. B Appl.* **2002**, *15*, 395–406.
25. Liao, S.M.; Zhao, T.S. An experimental investigation of convection heat transfer to supercritical carbon dioxide in miniature tubes. *Int. J. Heat Mass Transf.* **2002**, *45*, 5025–5034. [CrossRef]

26. Nano Nuclear Energy Inc. Nano Nuclear Energy. Available online: https://nanonuclearenergy.com/ (accessed on 15 December 2025).
27. Di Ronco, A.; Giacobbo, F.; Lomonaco, G.; Lorenzi, S.; Wang, X.; Cammi, A. Preliminary Analysis and Design of the Energy Conversion System for the Molten Salt Fast Reactor. *Sustainability* **2020**, *12*, 497. [CrossRef]